Solid State Phenomena
ISSN: 1662-9779, Vol. 390, pp 19-29
doi:10.4028/p-MDl8Q0

Submitted: 2025-12-18
Revised: 2026-02-17
Accepted: 2026-02-21
Online: 2026-04-17

Numerical Quantification of Structure-Property Relations in DP800 – Influence of Phase Material Models in RVE

Fehlemann Niklas C.[1,a*], Münstermann Sebastian[1,b]

[1]Institute of Metal Forming, RWTH Aachen University

[a*]niklas.fehlemann@ibf.rwth-aachen.de, [b]Sebastian.muenstermann@ibf.rwth-aachen.de

*Corresponding author

Keywords: dual phase steel, representative volume elements, damage, microstructure, sensitivity analysis, crystal plasticity.

Abstract. Understanding the relationships between (micro) structure and (mechanical) properties is inevitable for the design of modern structural metallic materials. A crucial property for most high-strength steels is ductile damage tolerance. Ductile damage in form of voids or microcracks can accumulate during cold forming, which either leads to failure in the forming process or subsequently affects the performance. Structure-property relations are often investigated using numerical methods, e.g. crystal plasticity (CP) modeling with statistically representative volume elements (sRVE). In a previous study, CP-simulations on 3D-sRVE were coupled with surrogate modeling techniques performing a variance-based sensitivity analysis. This analysis enables *quantitative* descriptions of the relationships between microstructure features with the damage tolerance, quantified by different indicators for individual damage mechanisms. To investigate the effect of the individual material models and the corresponding phase properties, 500 sRVE simulations were carried out with different CP-parameter sets and the damage tolerance was investigated in the present paper. All sets stem from the same DP800 but were calibrated with different approaches. Surrogate models were trained on the simulative database to calculate Sobol Indices (SI), which are a measure of how strong damage tolerance is affected by a particular microstructure feature. The SI are compared for the individual material models and damage indicators. The structure-property quantification is heavily influenced by the different material models, resulting in different values for the SI and a different order of the individual microstructure features. The main factor for the pronounced differences is the differently evolving mechanical phase contrast between ferrite and martensite.

Introduction

Establishing a mapping between process, structure, property and performance relationships is of crucial importance for the precise understanding of process chains and associated materials [1]. Since experimental investigations can consume a significant amount of resources to explore a larger space of different process parameters or microstructures, simulative and data-based methods are often used in this context, especially for structure-property mappings [2, 3]. An important advantage of numerical approaches is that individual parameters can be varied independently from the others, e.g. to show the singular effect of martensite banding on mechanical properties [4]. When numerical models are employed, a core piece is the material model used. In the case of microstructure-property relations, crystal plasticity (CP) models in conjunction with statistically representative volume elements (sRVE) are often used to map microstructure and mechanical properties. One of the most important mechanical property is the tolerance against initiation and evolution of ductile damage, since ductile damage can lead to failure during cold forming or can influence the final product properties [5].

In a previous study by the authors [6], a combined numerical and data-based structure-property quantification was carried out on a dual-phase steel DP800. Microstructural features like grain sizes and shapes were linked with damage tolerance using CP-simulations with a newly calibrated material model [7]. Based on a dataset of 250 virtual microstructure-damage pairs, surrogate modeling was employed to quantify the effect of the individual microstructure features on various damage

indicators. *However, the question of how the material models of the individual phases influences this structure-property quantification remained unanswered*. Therefore, the aim of this study is to conduct a second structure-property quantification with a different material model calibrated for the same steel in order to reveal the effect of the material model on structure-property quantification.

The general procedure is as follows: first, a dataset of sRVE of a DP800 with virtual microstructure concepts, i.e., for example, varying phase ratios or smaller or larger ferrite or martensite grains are generated. These sRVE are simulated with a second CP model for the same base DP800 and evaluated for their damage tolerance using different damage indicators for cleavage fracture of martensite or phase boundary decohesion. Based on this database of sRVE simulations, variance-based sensitivity analysis is performed with surrogate modeling to quantify the effect of the individual microstructure variation on the damage tolerance. Finally, the results for both CP-parameter sets are compared, and the differences are presented and discussed.

Materials & Methods

The methodology for the numerical and data-based structure-property quantification employed in this study closely resembles the approach presented in Fehlemann et al. [6], and as such, it will only be briefly summarized here.

Microstructure model.

The base material is a standard DP800 steel with a strongly heterogeneous microstructure made up of ferrite and martensite. The martensite is either present as small, irregular-shaped islands or larger, elongated bands and makes up about 30% of the material. For the generation of the sRVE, the open source sRVE generator DRAGen [8] is employed. DRAGen is especially good at capturing the heterogeneous, irregular microstructure of the DP800. In this study, seven different microstructural features and their respective effect on the damage are investigated, with the subsequently used abbreviations in brackets:

1. The phase ratio between ferrite and martensite (*P-R*)
2. The grain size of ferrite (*F_GrSize*)
3. The aspect ratio of the ferrite grains (*F_Ar*)
4. The island size of martensite (*M_GrSize*)
5. The aspect ratio of the martensite islands (*M_Ar*)
6. Binary variable indicating presence of martensite bands (*N_bands*)
7. The hardening of the ferrite phase (*f_hard*)

Details on how the variations are implemented in DRAGen and the material model can be found in [6]. It is important to note that the modifications on the microstructure are made in relation to the base microstructure. This means that a higher value for *F_GrSize* results in larger grains compared to the base material and vice versa. Example sRVE with different virtual microstructures are presented in Fig. 1.

Material model.

The aim of this study is the comparison of material model parameter sets and their effect on the structure-property quantification. Two sets of CP-parameters were utilized to investigate the influence of the material model and the associated mechanical (phase) properties on the effect of the microstructure features on damage tolerance. The first set (henceforth denoted as S_1), calibrated by Fehlemann et al. [7] and utilized for the study in [6] is based on *in situ* micropillar compression tests. The fundamental principle underlying this methodology for CP-calibration is based on the fact that the strain hardening measured in the *in situ* micropillar compression test *cannot* be directly transferred to the polycrystal, given that the strain hardening due to free surfaces in the micropillar differs from that in the polycrystal [9]. Consequently, the micropillar tests were milled from pre-strained macroscopic tensile specimens to estimate the hardening of the polycrystal via the change in CRSS at different pre-strain levels. The parameters for the martensite can be fitted directly from the micropillar compression tests, since the martensite contains enough interfaces to closely resemble

bulk behavior [10]. S_1 also considers grain size effects with a Hall-Petch type scaling law as well as the effect of the carbon content on the martensite hardness.

The second set (S_2) is derived from Pütz et al. [11]. In this case, the calibration of the CP-parameters for the ferrite was achieved using nanoindentations, whereby the force-indentation curves for individual grains were fitted. Subsequently, the model parameters for the martensite were inversely fitted to the homogenized true stress-strain curve of the bulk material. An optimal fit for the martensite is reached when the homogenized stress-strain curve from the DP800 sRVE closely resembles the homogenized true stress-strain curve of the bulk material. Since the structure-property pairs for the first set are taken from Fehlemann et al. [6], only simulations with S_2 are carried out in this study. All simulations in this paper are carried out with the open-source multiphysics framework DAMASK [12].

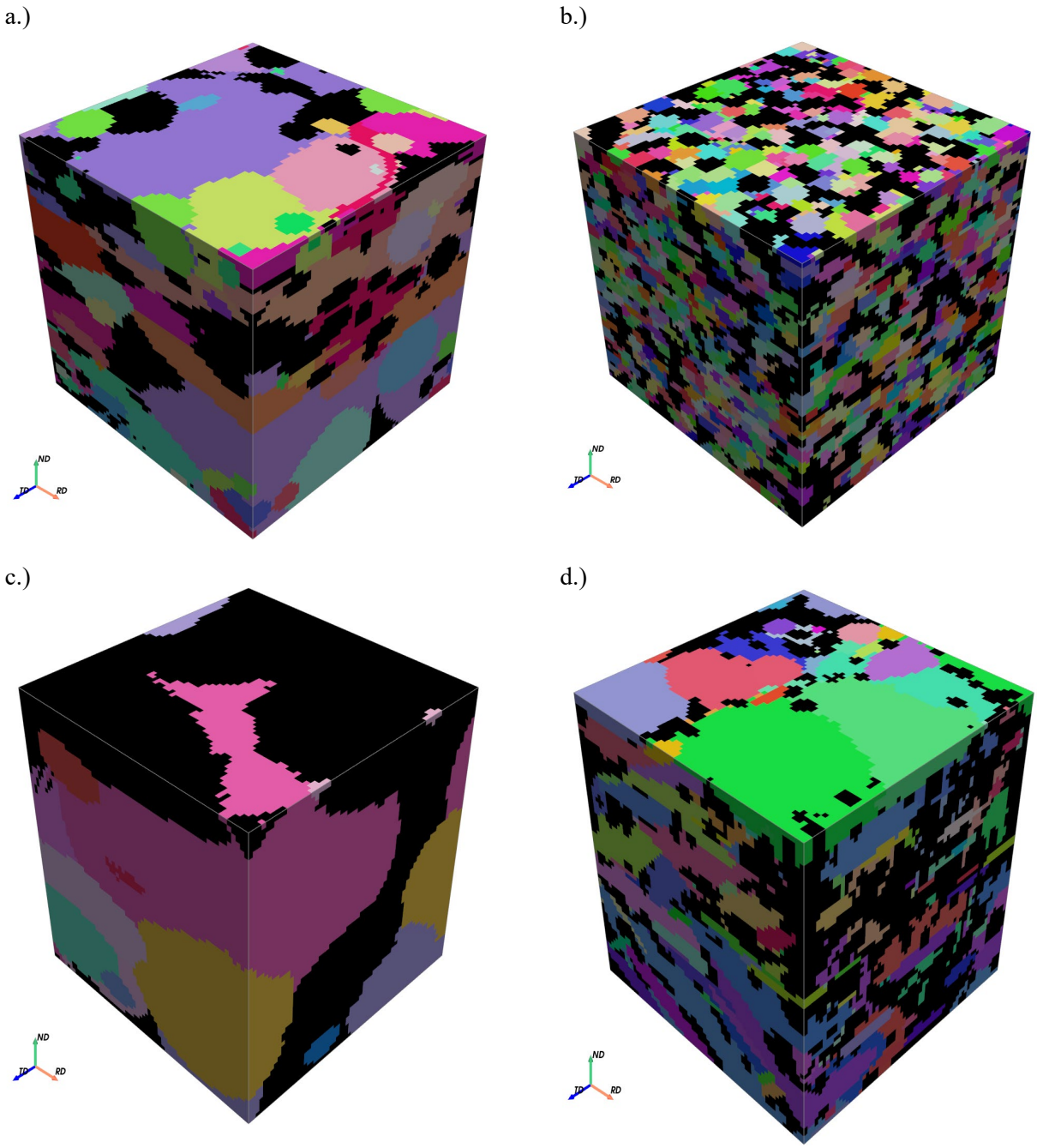

Fig. 1. Example sRVE with virtual microstructures. a.) Base microstructure, b.) fine grained ferrite and martensite, c.) Coarse ferrite and martensite, d.) ferrite elongated in RD plus fine-grained martensite.

Damage indicators

As in [6], three damage indicators are used for the most common ductile damage mechanism in DP-steels. It should be noted that the indicators are only for damage initiation, since there is no damage model to predict the evolution of damage during plastic deformations. All indicators are calculated solely from the stress- and strain fields after the simulation has finished. The first indicator for cleavage fracture of martensite (denoted as Ind_C, indicator for cleavage fracture) is determined by the percentage of elements in an sRVE that exceed a specified threshold of the maximum principal stress. The value for the principal stress is derived using the methodology by Steinbrunner et al. [13]. According to their findings, the fracture of martensite occurs at approximately 5% strain, which corresponds to a stress threshold of 3500 MPa for S_1 and 1350 MPa for S_2. The difference stems from the different material parameters for martensite in the two sets. To assess the damage initiation by phase boundary decohesion, a novel indicator was developed. This indicator is based on the magnitude and scatter of the equivalent plastic strains at the interfaces between ferrite and martensite. The indicator is denoted as Ind_{PBD} (Indicator for phase boundary decohesion), and further details can be found in [6]. As an additional measure of the overall damage tolerance, an equally weighted normalized average of Ind_C and Ind_{PBD} is calculated, which is referred to as Ind_H (Homogenized indicator). Furthermore, it was decided not to use an indicator for damage initiation in ferrite grains, as this rarely occurs in the DP800 under consideration [14, 15].

Structure-property quantification.

In order to calculate the aforementioned Sobol indices [16], surrogate modeling approaches are required, since SI cannot be calculated directly from the numerically generated database itself. SI are a measure of the fraction of the variance of the output of a given system caused by a specific input feature. Thus, they are a measure of how important a specific input feature is [17]. To mitigate the effect of the surrogate modeling strategy, two different model classes are used with different hyperparameters. Gaussian Process Regression (GPR) [18] is used with three different kernels, while Polynomial Chaos Expansion (PCE) [19] is used with two different forms of the underlying distributions. All five surrogate models are trained on the simulative database, and the SI are calculated from the trained models. It is noteworthy that the calculation process of the SI is different for both PCE and GPR. For PCE, the SI can be directly derived from the model parameters [19]; for GPR, they are calculated by sampling from the model in a specific manner [17]. Therefore, the SI shown in this paper are the average over the five models. The database consists of 250 virtual microstructure concepts from the aforementioned 7d design space. To reduce the scatter, 2 sRVE are simulated for each microstructure concept, yielding 500 sRVE simulations in total. The load case is uniaxial tension along the rolling direction (RD) until 12% global strain, shortly before the uniform elongation of the base material.

Results

Material model comparison.

The global, homogenized true stress-strain curves for both parameter sets are presented in Fig. 2, alongside the experimental true stress-strain curve from the uniaxial tensile tests. It is evident that both parameter sets demonstrate a strong agreement with the experimental data. For S_1, the prediction quality for low strains, up to 0.06, is particularly excellent, with subsequent minor deviations. For S_2, the trend is opposite, with small overestimations at the beginning and a good fit for higher strains. It can be stated that, in general, both fits are adequate, particularly when taking into consideration the complexity of micromechanical modeling of multiphase materials.

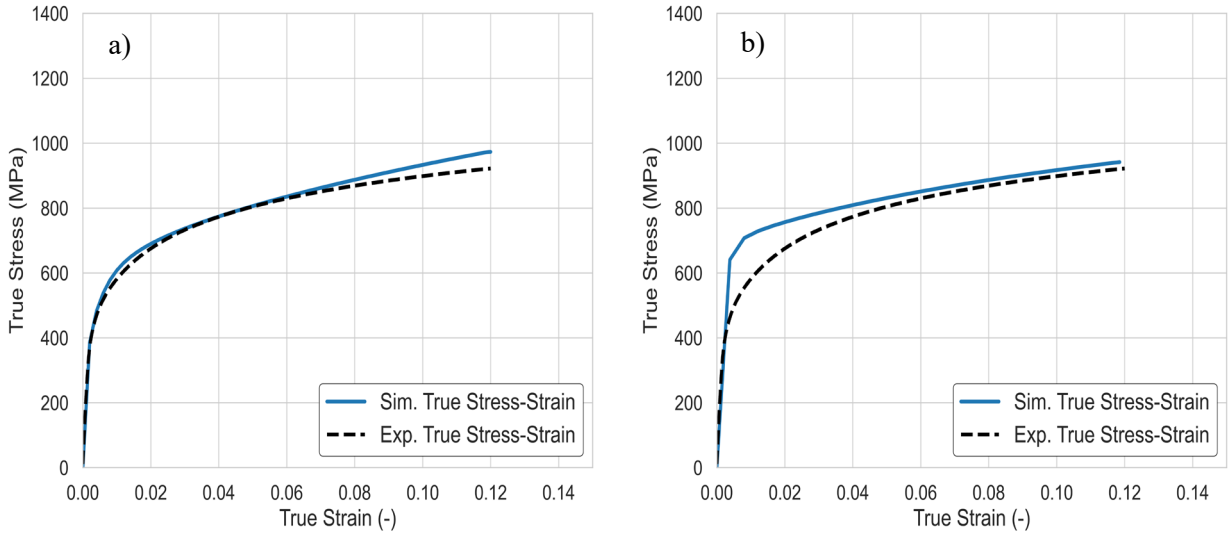

Fig. 2. Comparison of simulative (solid blue) and experimental (dashed black) true stress – strain curves for the parameter sets S_1 (a) and S_2 (b).

In addition to the homogenized true stress – strain curves, the individual strain hardening curves for both phases are shown in Fig. 3. Fig. 3a depicts the CRSS of the ferrite, while Fig. 3b shows the true stress-strain curves for the martensite. A pronounced strength difference is observable for martensite: while the yield stress for S_1 is around 3000 MPa, it is only around 800 MPa for S_2. On the other hand, S_2 shows a more pronounced strain hardening of martensite. For the ferrite, the trend is vice versa, since the strain hardening is more pronounced for S_1. A direct comparison between S_1 and S_2 in terms of the yield strength is not straightforward, as the values for S_1 are skewed by the incorporated grain size scaling effects.

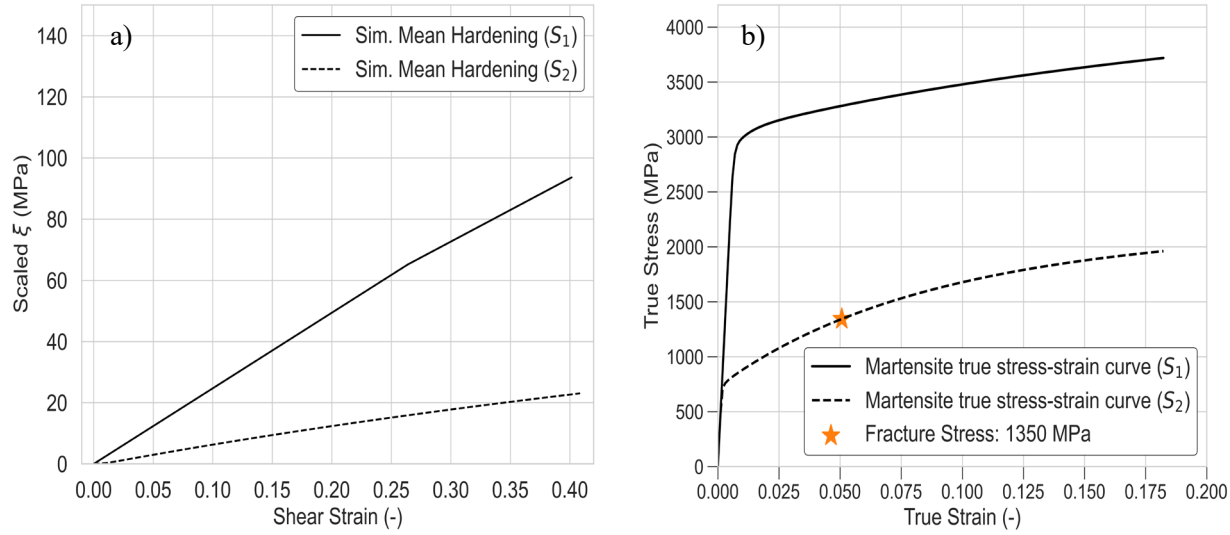

Fig. 3. Comparison of material models S_1 and S_2 in terms of phase properties. a.) scaled ferrite hardening, b.) martensite true stress – strain curves.

Best and worst microstructures.

Before evaluating the surrogate models and computing the structure-property quantification by means of the SI, the optimal and critical microstructures are derived directly from the numerical dataset of virtual microstructure-damage pairs. To circumvent the overestimation of potential outliers, the 250 data points for each indicator are sorted, and the 95th and 5th percentiles are calculated. The mean value of the individual microstructure features is subsequently determined and designated as the "optimal" or "critical" microstructure. These are represented in the radar charts in Fig. 4, alongside the respective microstructures for S_1, taken from [6]. The microstructure of the base material is also

plotted for comparison. The rows show the three damage indicators, with the optimal microstructure configurations on the left side and the critical on the right side. All arms are normalized in the interval $I \in [0,1]$.

Optimal microstructures

Critical microstructures

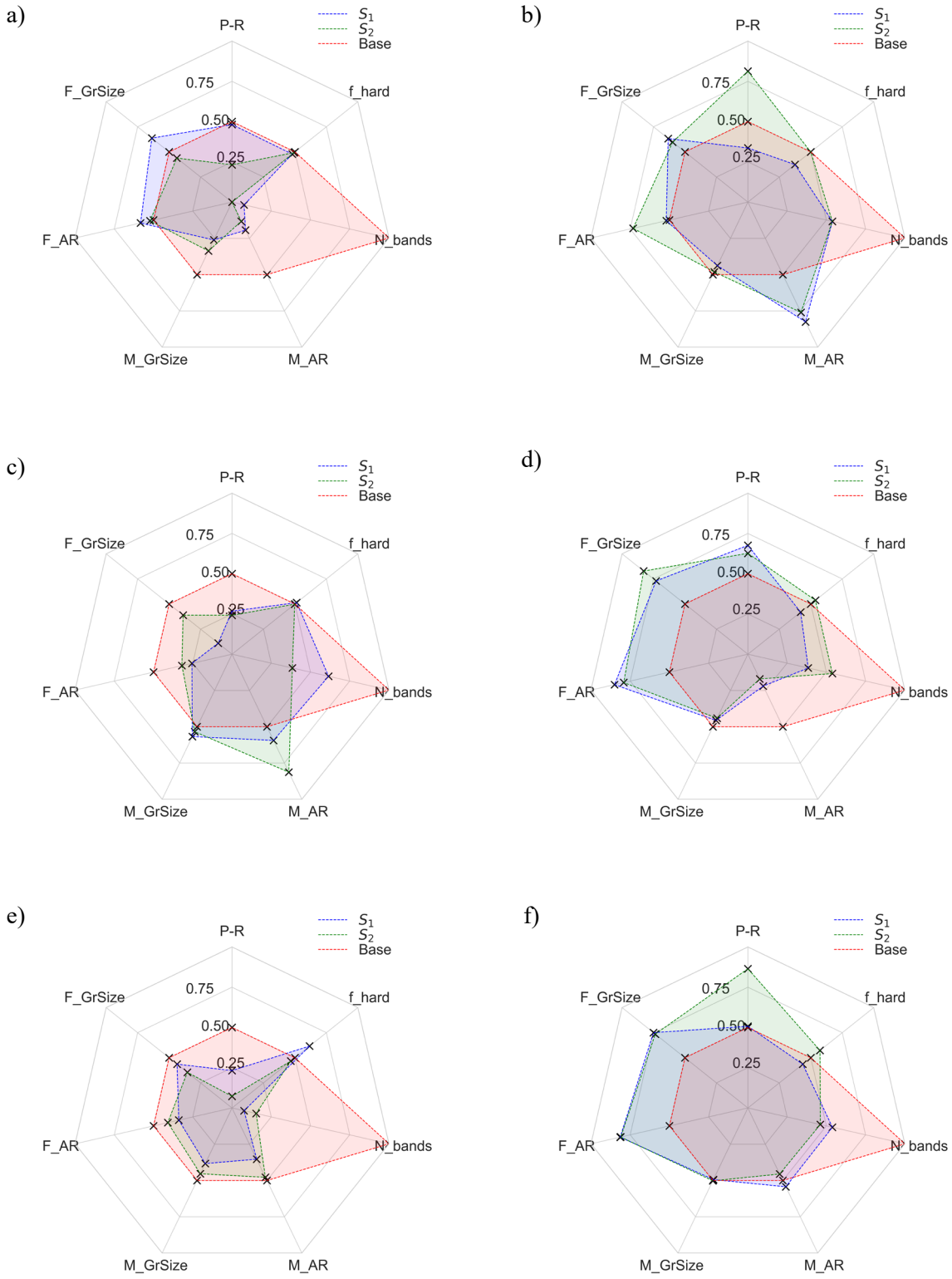

Fig. 4. Radarcharts showing the optimal (left) and critical (right) microstructures for all three indicators. Upper row: IndC, middle row: IndPBD, lower row: IndH.

The discrepancies between S_1 and S_2 are comparatively small for a same load case. For Ind_B in the initial row, the absence of bands and the elongation of martensite perpendicular to the loading direction (low values for *M_ar*) are advantageous, which strongly deviates from the base microstructure, which exhibits more elongated martensite and pronounced banding. A visible discrepancy between S_1 and S_2 is observed for the phase ratio, where S_2 predicts more martensite to be critical, whereas S_1 predicts a lesser amount of martensite to be critical (Fig. 4b). For Ind_{PBD}, particularly the critical microstructures are highly analogous (Fig. 4d). For the optimal microstructure, deviations are evident for the ferrite grain size and the bands. The radar charts for Ind_H (Fig. 4e) reveal that both models suggest relatively small values for all microstructure features to be optimal. A notable discrepancy is once again evident for the phase ratio for the critical microstructure configurations (Fig. 4f), where a medium amount of martensite is predicted to be critical in S_1, compared to a high amount of martensite for S_2.

Surrogate Model quality.

The set of 250 virtual microstructure-damage pairs was utilized to train the five surrogate models (2x PCE, 3x GPR). Prior to the calculation of the SI from the models, it is imperative to evaluate their prediction quality, as a bad model will most likely produce wrong or at least imprecise SI. The coefficient of determination (R^2) serves as the primary metric for model quality. This measure is preferable to the mean squared error (MSE), as it would overestimate errors for higher values of the damage indicators. The results are presented in Fig. 5, where the predictions and ground truth values are compared. The GPR predictions are located on the left side, while the PCE predictions are depicted on the right. It is evident that the model quality is generally very good, with R^2-values ranging between 0.75 – 0.9. Graphically, the good model prediction is underlined by the fact that all values lie closely along the blue ideal line. The 95%-confidence interval (shaded) computed directly from the residuals $y_{true} - y_{pred}$ is relatively narrow, which is also an indicator of good model quality. Overall, the GPR predictions are superior to the PCE predictions, a trend that holds true for all three damage indicators. In contrast, no significant differences are observed among the indicators. If substantial deviations between the prediction and the ground truth occur, they are predominantly underestimations of large ground truth values, i.e. they occur on the right-hand side of the graphic and right to the ideal line. Therefore, residuals that fall out of the confidence interval predominantly occur on this side of the ideal line.

Structure property quantification.

In Fig. 6, the SI are displayed. The original SI from [6], determined using the material model S_1, are slightly shaded, while the new SI, as determined in this study based on the S_2 CP model, are darker blue. For the brittle indicator Ind_B, the phase ratio (*P-R*) shows a significantly increased effect (0.1 → 0.55), while the influence of all microstructural morphology features, particularly the martensite aspect ratio, is reduced. For the ductile indicator Ind_{PBD}, the impact of the martensite aspect ratio is increased, while both grain size effects are reduced. For the ferritic phase, this can be attributed to the absence of Hall-Petch type grain size scaling effects in the S_2 model, which should clearly diminish the effect of the grain size. In contrast to Ind_B, the phase ratio's effect is slightly decreased rather than increased. Finally, the effects of both aspect ratios are interchanged for the homogenized indicator Ind_H: the effect of the ferrite aspect ratio is increased, and the effect of the martensite aspect ratio is decreased. All other features remain largely unaffected by the material model change.

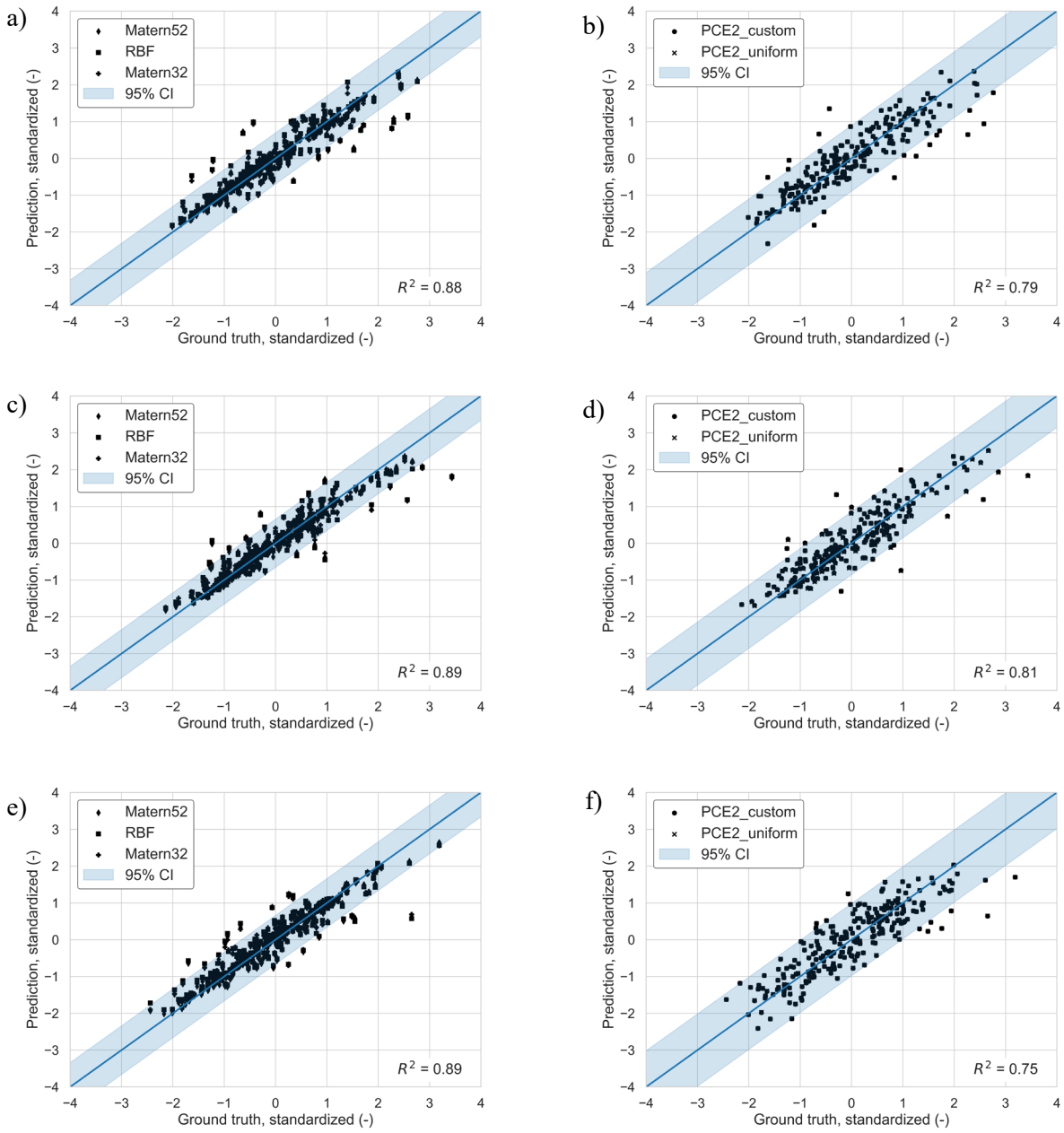

Fig. 5. Model quality estimation. (a), (c), (e) show the GPR-predictions, (b), (d), (f) the PCE predictions. The shaded area denotes the confidence interval based on the residuals. (a) and (b) Cleavage indicator, (c) and (d) PBD-indicator, (e) and (f) Homogenized indicator.

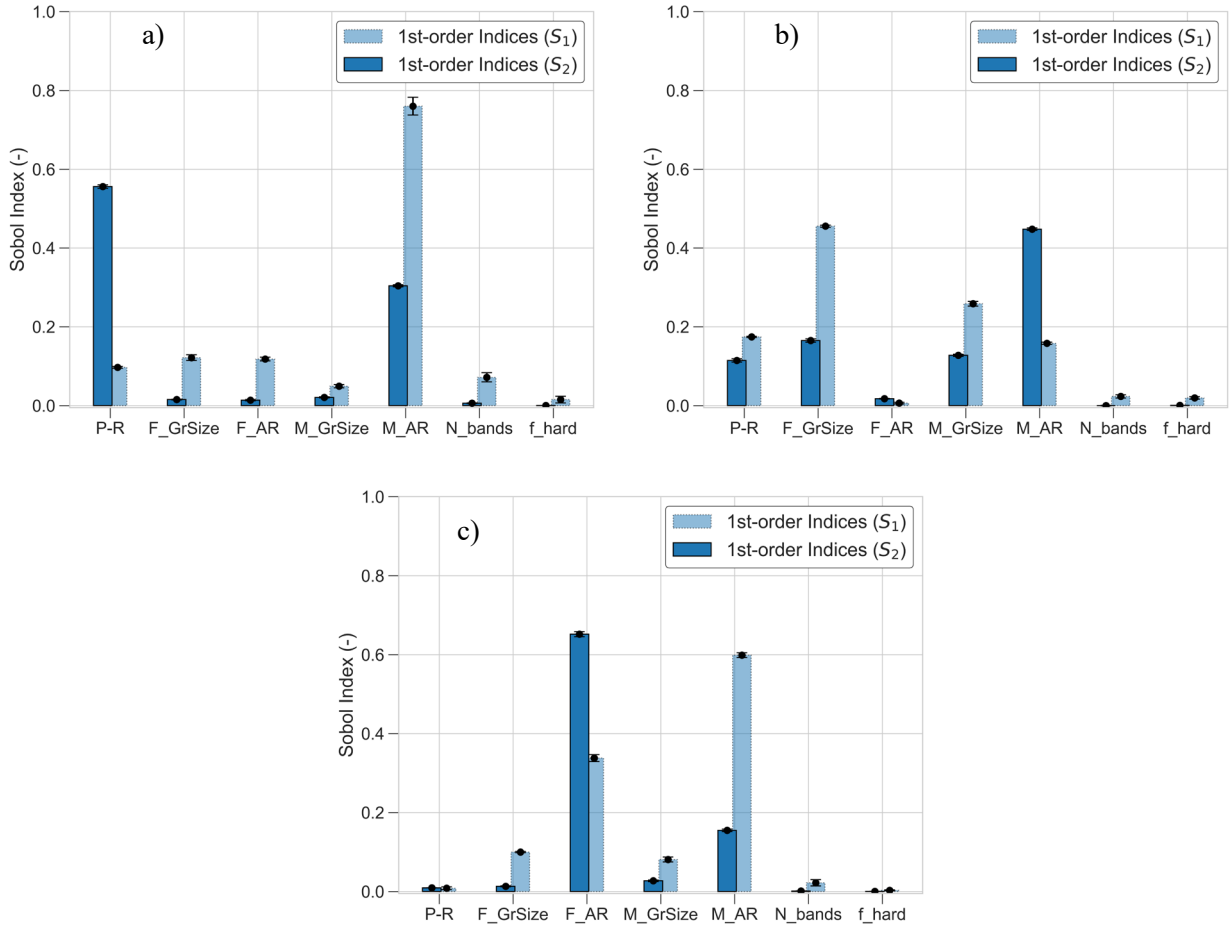

Fig. 6. Comparison of the SI based on the two different material models. a.) Ind_C, b.) Ind_{PBD}, c.) Ind_H.

Discussion

Comparing the structure-property quantifications with two different material models reveal pronounced differences between optimal and critical microstructures as well as the SI. Since all other parameters of the studies, such as the feature space and RVE size, are equal, the differences must stem from the parameter sets. The differences in the calibration approach, especially the difference in the micromechanical data used, result in significant discrepancies. First, only the S_1 model is really validated, since the S_2 model uses the macroscopic true stress-strain curve for inverse calibration of the martensite phase. Consequently, potential errors in calibrating the CP parameters of the ferrite can be offset in the martensite calibration and still result in a good overall fit of the homogenized true stress-strain curve from the uniaxial tensile tests, as shown in Fig. 2. Furthermore, calibrating the ferrite using nanoindentations depends on the target value [20]. In literature, the force-indentation curve, post-mortem imprint, or pile-up topography is used, all with their own (dis)advantages. Fig. 3 shows that the S_2 model would likely predict the micropillar compression for ferrite and martensite incorrectly, since it underestimates the ferrite hardening, while simultaneously overestimating the martensite hardening, although the yield stress of the martensite is also strongly underestimated by S_2. Therefore, it can be concluded that the S_2 parameter set models the phase contrast between ferrite and martensite smaller than the S_1 model, caused by weaker martensite and presumably stronger ferrite without the grain size effects. The fact that the homogenized stress-strain curve is nevertheless predicted correctly is due to the inverse calibration of the martensite and the lack of validation.

The exact reasons behind the differences in the SI between S_1 and S_2 are beyond the scope of this study. It is assumed that due to the presumably higher fidelity of the S_1 model (as discussed before), the S_1 SI are closer to reality. Since it can be concluded that the S_2 model is at least inaccurate, if not

downright wrong (since it will fail on predicting the micropillar compression experiments), the SI are also not trustworthy. This therefore underscores the need for a highly accurate material model if a structure-property quantification or a computational microstructure optimization is planned. Not only are the levels of the SI nearly completely different, but also the order of the different indices is perturbed. This underlines the importance of a correct modeling of the individual phase properties and the associated evolution of the mechanical phase contrast for a precise damage assessment.

Summary

In this study, a numerical and data-based structure-property quantification approach was employed to establish a correlation between microstructural features and ductile damage tolerance of a DP800 steel. The results were then compared to those of a similar study that employed a differently calibrated material model. This comparison was undertaken to investigate the influence of the material model parameter set on the structure-property quantification. A pronounced effect was observed, with both the values and the order of the SI being significantly different. The underlying reason for this discrepancy is presumed to be the differently modelled evolution of the mechanical properties in both models S_1 and S_2, which consequently leads to diverging predictions of ductile damage behavior. This highlights the necessity for precise calibration and validation of the material models and the right choice of the experimental database for calibration. Furthermore, the extent to which the material model affects other variables, apart from damage initiation, such as global formability or effective stiffness, should be investigated.

Acknowledgement

This research was funded by Deutsche Forschungsgemeinschaft (DFG, German Research Foundation; Projectnumber 278868966 – TRR 188; Damage Controlled Forming Processes, subproject B05). The simulations were carried out with computing resources granted by RWTH Aachen University under project rwth1645.

References

[1] A. Agrawal and A. Choudhary, Perspective: Materials informatics and big data: Realization of the “fourth paradigm” of science in materials science. APL Materials, 5 (2016).

[2] J. Jung, J. I. Yoon, H. K. Park, J. Y. Kim, and H. S. Kim, Bayesian approach in predicting mechanical properties of materials: Application to dual phase steels. Materials Science and Engineering: A (2019) 382–390.

[3] N. Kusampudi and M. Diehl, Inverse design of dual-phase steel microstructures using generative machine learning model and Bayesian optimization. International Journal of Plasticity (2023) 103776.

[4] E. E. Aşık, E. S. Perdahcıoğlu, and T. van den Boogaard, An RVE-Based Study of the Effect of Martensite Banding on Damage Evolution in Dual Phase Steels. Materials (Basel, Switzerland), 7 (2020).

[5] A. E. Tekkaya, N. Ben Khalifa, O. Hering, R. Meya, S. Myslicki, and F. Walther, Forming-induced damage and its effects on product properties. CIRP Annals, 1 (2017) 281–284.

[6] N. C. Fehlemann, I. Biermann, and S. Münstermann, Exploring structure–property relations in dual phase steels using crystal plasticity and variance based global sensitivity analysis. Materials & Design (2025) 114794.

[7] N. C. Fehlemann, A. Medina, S. Lee, C. Kirchlechner, and S. Münstermann, Crystal plasticity parameter identification via statistical relevant micropillar compression. Acta Materialia (2025) 121321.

[8] M. Henrich, N. Fehlemann, F. Bexter, M. Neite, L. Kong, F. Shen, M. Könemann, M. Dölz, and S. Münstermann, DRAGen - A deep learning supported RVE generator framework for complex microstructure models. Heliyon, 8 (2023) e19003.

[9] G. Dehm, B. N. Jaya, R. Raghavan, and C. Kirchlechner, Overview on micro- and nanomechanical testing: New insights in interface plasticity and fracture at small length scales. Acta Materialia (2018) 248–282.

[10] H. Ghassemi-Armaki, P. Chen, S. Bhat, S. Sadagopan, S. Kumar, and A. Bower, Microscale-calibrated modeling of the deformation response of low-carbon martensite. Acta Materialia, 10 (2013) 3640–3652.

[11] F. Pütz, N. Fehlemann, V. Göksu, M. Henrich, M. Könemann, and S. Münstermann, A data driven computational microstructure analysis on the influence of martensite banding on damage in DP-steels. Computational Materials Science (2023) 111903.

[12] F. Roters, M. Diehl, P. Shanthraj, P. Eisenlohr, C. Reuber, S. L. Wong, T. Maiti, A. Ebrahimi, T. Hochrainer, H.-O. Fabritius, S. Nikolov, M. Friák, N. Fujita, N. Grilli, K. Janssens, N. Jia, P. Kok, D. Ma, F. Meier, E. Werner, M. Stricker, D. Weygand, and D. Raabe, DAMASK – The Düsseldorf Advanced Material Simulation Kit for modeling multi-physics crystal plasticity, thermal, and damage phenomena from the single crystal up to the component scale. Computational Materials Science (2019) 420–478.

[13] D. L. Steinbrunner, D. K. Matlock, and G. Krauss, Void formation during tensile testing of dual phase steels. Metall Trans A, 3 (1988) 579–589.

[14] C. Kusche, T. Reclik, M. Freund, T. Al-Samman, U. Kerzel, and S. Korte-Kerzel, Large-area, high-resolution characterisation and classification of damage mechanisms in dual-phase steel using deep learning. PloS one, 5 (2019) e0216493.

[15] C. F. Kusche, F. Pütz, S. Münstermann, T. Al-Samman, and S. Korte-Kerzel, On the effect of strain and triaxiality on void evolution in a heterogeneous microstructure - A statistical and single void study of damage in DP800 steel. Materials Science and Engineering: A (2021) 140332.

[16] I. Sobol′, Global sensitivity indices for nonlinear mathematical models and their Monte Carlo estimates. Mathematics and Computers in Simulation, 1-3 (2001) 271–280.

[17] M. Böddecker, M. Faes, A. Menzel, and M. A. Valdebenito, Effect of uncertainty of material parameters on stress triaxiality and Lode angle in finite elasto-plasticity—A variance-based global sensitivity analysis. Advances in Industrial and Manufacturing Engineering (2023) 100128.

[18] C. E. Rasmussen and C. K. I. Williams (2005. *Gaussian Processes for Machine Learning*. The MIT Press.

[19] R. Ghanem, D. Higdon, and H. Owhadi (2017. *Handbook of Uncertainty Quantification*. Springer International Publishing, Cham.

[20] F.-J. Gallardo-Basile, F. Roters, R. M. Jentner, J. P. Best, C. Kirchlechner, K. Srivastava, S. Scholl, and M. Diehl, Application of a nanoindentation-based approach for parameter identification to a crystal plasticity model for bcc metals. Materials Science and Engineering: A (2023) 145373.

The publication of this article was funded by the RWTH Aachen University 10.13039/501100007210